

Research papers

Urea nitrogenated mesoporous activated carbon derived from oil palm empty fruit bunch for high-performance supercapacitor

Heri Rustamaji^{a,b}, Tirto Prakoso^{a,*}, Hary Devianto^a, Pramujo Widiatmoko^a,
Wibawa Hendra Saputera^a

^a Department of Chemical Engineering, Bandung Institute of Technology, Jl. Ganesha 10, Bandung 40132, Indonesia

^b Department of Chemical Engineering, Lampung University, Jl. Soemantri Brojonegoro No.1, Bandar Lampung 35145, Indonesia



ARTICLE INFO

Keywords:

Biomass
Hydrothermal carbonization
Mesoporous activated carbon
Energy storage
Supercapacitor

ABSTRACT

This study aims to synthesize urea nitrogenated activated carbon (N-ACU) derived from oil palm empty fruit bunches and examine its performance as a supercapacitor electrode. The synthesis was carried out in three stages: hydrothermal carbonization with CaCl_2 activator, impregnation with urea, and activation of nitrogenated hydrochar with CO_2 gas. The urea to hydrochar impregnation ratio was varied by weight at 1, 2, and 3, while physical characterization of the material was carried out by SEM, XRD, adsorption/desorption isotherms, and FTIR. Porosity analysis showed that all the samples had a mesoporous structure with 3.3–5.8 nm and a BET surface area of 363.88–640.61 $\text{m}^2 \text{g}^{-1}$. Furthermore, the electrochemical characterization indicated that the optimum result was obtained for the N-ACU3 sample with an electrode-specific capacitance value of 176.76 F g^{-1} at a scan rate of 2 mV s^{-1} . The highest energy and power density values at the current of 1 A g^{-1} were 19.89 Wh kg^{-1} and 1431.20 W kg^{-1} , respectively. Durability tests of supercapacitor carried out by cyclic charge-discharge for 5000 cycles showed that the coulombic efficiency and capacitance retentions were approximately 100% and 98.7%, respectively. Based on the results, the urea to hydrochar impregnation ratio affects the characteristic of N-ACU and the performance of supercapacitors. In addition, urea nitrogenated treatment on activated carbon can reduce the ohmic and charge transfer resistance and maintain the supercapacitor's cell stability. The improved supercapacitor performance indicates that the Synthesis of nitrogenated activated carbon from biomass waste can be a promising method for producing electrode materials.

1. Introduction

As the demand for clean, long-term energy solutions increases, supercapacitors have gained substantial attention due to their rapid charge/discharge rates, high power density, fantastic cycling stability, and low production costs [1–3]. Carbon with pores has recently been recognized as a top supercapacitor electrode material due to its remarkable properties, such as wide surface area, high conductivity of electricity, and vigorous stability in both physical and chemical terms [4,5]. However, the intricate microporous architectures and disordered textures, leading to the presence of a long diffusion distance and a high barrier to ion transfer, cannot promptly meet the growing need for high-performance supercapacitors at high current densities [6]. Supercapacitors made of pure carbonaceous materials also have poor energy density and low specific capacitance, which limit their usage [7]; hence several efforts have been carried out to develop high-performance

supercapacitors using carbon-based electrodes. The electrode material for electrical double layer capacitance (EDLC) needs chemical stability, excellent electrical conductivity, a large surface area, and a regulated pore design. [5]. Pseudocapacitance emerging from some oxides and hydroxides of transition metals has also been studied in EDLC. For example, the oxides/hydroxides of transition metals and conducting polymers are two of the most common ways to improve pseudocapacitance in supercapacitors [8]. However, some significant limitations, such as the transition metal oxides' low conductivity of electricity, high price, and the conductive polymers' insufficient cycle stability, limit their widespread application [9,10]. The method of adding heteroatoms such as B, N, O, P, and S with porous carbon frameworks to generate new carbon compounds and improve the pseudocapacitance effect has attracted massive attention [11]. Charge transfer by pseudocapacitance is achieved by enhancing the basicity of the carbon electrode material and the electron donors by nitrogen atoms in the event of nitrogen (N)-

* Corresponding author.

E-mail address: tirto@che.itb.ac.id (T. Prakoso).

<https://doi.org/10.1016/j.est.2022.104724>

Received 25 February 2022; Received in revised form 13 April 2022; Accepted 20 April 2022

Available online 30 April 2022

2352-152X/© 2022 Published by Elsevier Ltd.

doping. Electrical conductivity can also be improved by doping nitrogen into carbon, thereby allowing more mobility of charge/electron carriers [12]. In carbon-based materials, nitrogen affects the porosity properties including the average pore size and distribution, specific surface area, total pore volume, as well as acts as an electron donor [13].

Given the possible scope of supercapacitor applications and the shortage of fossil energy, the use of biomass wastes and renewable biomass to make carbon-based materials with specific nanoarchitectures in the energy field is considered worthwhile and is gaining massive attraction [14,15]. Porous carbons have been made from various agricultural wastes, including corn cobs and stalks, rice husks, coconut shells, bagasse, palm shell, and others, using activating agents such as H_3PO_4 , KOH, and $ZnCl_2$ for activation methods [6]. Oil palm empty fruit bunch (OPEFB) is a bountiful and free renewable agricultural lignocellulose byproduct derived from palm oil. It is produced in Indonesia at a rate of 40 million tons per year and used traditionally as a fertilizer after burning, a substance for mulching plantations of palm oil, and palm oil mill boiler fuel [16]. Particleboard, medium-density fiberboard, and bedding materials are examples of non-traditional usage. This biomass waste is also an effective precursor for synthesizing porous carbons using the activating agent of KOH, $ZnCl_2$, H_3PO_4 , and calcination [17]. Some of the porous as-prepared carbons have a capacitance suitable for supercapacitors. Furthermore, several studies on the synthesis of activated carbon for supercapacitors from OPEFB have been carried out [18–21]. Using biomass or its waste as precursors is sustainable to manufacture porous carbons for supercapacitors. However, due to their low nitrogen content, most as-prepared carbons have a medium-specific capacitance which prevents optimal use in high energy density supercapacitors. In this case, bulk manufacturing of porous carbons with a high nitrogen content derived from biomass waste pyrolysis under various experimental settings is an effective technique to increase the gravimetric capacitance of their devices [22].

KOH and $ZnCl_2$ as activating agents have been suggested to enhance surface area and increase the pore structure while drastically lowering the N content of carbon-based materials as-prepared [23]. Meanwhile, the application of activating agents might have greater or lesser severity drawbacks, such as solid instrument and equipment corrosion and a high level of toxicity and expenses, which will limit their broad and practical use or raise the cost of manufacturing in large quantities. Therefore, obtaining carbons from low-cost, sustainable biomass waste containing high nitrogen concentration, large specific surface area, and supercapacitors with good performance using an environmentally friendly technique is challenging [1,6,24].

The production of porous carbon as an adsorbent from waste biomass by chemical activation using $CaCl_2$ as a substitute for KOH and $ZnCl_2$ has been explored [25]. However, investigations into the synthesis of nitrogenated porous carbons that utilize activating agent of $CaCl_2$ are rare. The synthesis of N-enriched porous carbons from biomass wastes such as OPEFB using $CaCl_2$ at suitable hydrothermal carbonization and activation condition is presumably a cheap, renewable, effortless, and ecologically conscious strategy. Therefore, this research aims to synthesize activated carbon with hydrothermal carbonization of $CaCl_2$ activation agent, urea nitrogenated modification, and pyrolysis activation as an alternative method by emphasizing a study on the effect of impregnation ratio on physical-chemical properties and electrochemical properties. The research finding is that the modification of activated carbon from OPEFB with urea can increase the wettability, conductivity, and specific surface area, which improves the supercapacitor's performance compared to activated carbon without modification. The synergistic effects of $CaCl_2$ and urea on the porosity framework and nitrogenated activated carbons were also extensively studied.

2. Materials and methods

2.1. Material and solution

The biomass sample was oil palm empty fruit bunches (OPEFB) obtained from a local palm oil mill in Cikasungka, Bogor, Indonesia. Chemical reagents consisting of calcium chloride ($CaCl_2$, Merck, 99%), potassium hydroxide (KOH, Merck, 99%), hydrochloric acid (HCl, Merck, 99%), and urea ($CO[NH_2]_2$, Merck, 99%) were supplied by Merck, while ethanol (C_2H_5OH , AR, 96%), carboxymethylcellulose (CMC, 60%), and polyvinylidene fluoride (PVDF, 65%) were purchased from PT Bratachem, Bandung Indonesia. Furthermore, Whatman filter paper (Grade 40) used as an electrode separator was obtained from Sigma-Aldrich, while coin cell CR2032 for supercapacitor casing and crimping cell machine were purchased from Xiamen TOB New Energy, Fujian, China.

2.2. Synthesis nitrogenated porous activated carbon

The OPEFB biomass was washed, dried, and milled in 40 to 80 mesh diameters, and then it was pretreated for 2 h with a 1 M HF solution to remove ash. Filtered samples were dried in a 105 °C oven for 24 h. In the batch reactor, biomass and the activating agent solution were added to start the hydrothermal carbonization process, and the reaction occurred at a temperature of 275 °C for 1 h. After cooling through the sampling valve, the gaseous product was removed with the sampling bag. The mixture produced was collected and filtered to separate the solid and liquid portions, termed hydrochar and bio-oil, then the product was dried at 110 °C overnight [20,21].

Nitrogen doping was carried out by mixing urea with hydrochar in a ratio of 1, 2, and 3 in deionized water. Then a magnetic stirrer was used to agitate the mixture at 80 °C for 2 h. The hydrochar-urea mixture was evaporated and dried at 80 °C for 2 h. Subsequently, the hydrochar was activated by depositing on a ceramic boat in a tubular reactor and increasing the operating temperature to 800 °C at a thermal rate of 10 °C min^{-1} with a volumetric rate of 50 mL min^{-1} of N_2 . The N_2 gas stream was replaced with CO_2 at a 50 mL min^{-1} rate for 2 h, and then the reactor was cooled using N_2 gas when it was turned on. The activated carbon product was washed with 1 M HCl, neutralized with demineralized water, and filtered to eliminate any remaining $CaCl_2$ components. The nitrogenated activated carbon was produced after 2 h of drying at 105 °C [21]. Undoped activated carbon is represented by ACO, while urea doped activated carbon is represented by N-ACUX, where X is the urea to the hydrochar ratio.

2.3. Physical characterizations

Activated carbon's morphology and element content was characterized by Scanning Electron Microscope and Energy Dispersive Spectroscopy (SEM-EDS) using SEM Hitachi SU3500 carried out in Nano Center Research of Bandung Institute Technology (ITB). A Quantachrome TouchWin™ v1.2 was used to measure nitrogen adsorption/desorption of samples in the Instrumentation Laboratory of Chemical Engineering-ITB. The Brunauer–Emmett–Teller (BET) technique was used to compute the specific surface area, while the total pore volume was determined at a relative pressure of 0.9 using the adsorption amount. Furthermore, the Barrett–Joyner–Halenda (BJH) method was used to compute the pore size distributions (PSD), while the activated carbon crystal structure was established using a powder X-ray diffraction pattern (40 kV, 40 mA) with Bruker D8 advanced diffractometer and monochromatized Cu–K radiation [13]. The Raman spectra were obtained using an XploRa Plus Raman spectrophotometer with a 532 nm blue laser beam, and the qualitative assessment of OFGs was performed using Fourier Transform-Infrared (FTIR) analysis. The infrared vibrational mode of the samples was accepted at an average of 24 sweeps by a Nicolet 6700 FTIR spectrometer ranging from 5000 to 400 cm^{-1} with unearthly reach at 4 cm^{-1}

goals, and as well as a KBr pellet as a perspective example.

2.4. Electrochemical characterization

The electrode material consisted of activated carbon and 10 wt% PVDF (polyvinylidene fluoride). The powders were dispersed in ethanol and mixed by sonication for 30 min, then 0.2 g of the dry composite mixture was molded and pressed at 7–10 MPa to obtain a circle electrode with a diameter of 15 mm and thickness of 1 mm. A coin cell (CR2302) type supercapacitor was created with symmetrical 2.3 mg cm⁻² mass loading electrodes. The Whatman filter paper was used to separate the two electrodes in an aqueous electrolyte containing 6 M KOH, and then the cell was pressed by a hydraulic crimping machine. Moreover, the electrochemical behavior of the cell was characterized using a potentiostat (Gamry R3000) with a two-electrode system consisting of cyclic voltammetry (CV), galvanostatic charge-discharge (GCD), and electrochemical impedance spectroscopy (EIS) measurement. EIS studies were performed at an open-circuit voltage and various bias potentials with a range of frequencies from initial and end values of 100 kHz and 0.01 Hz, respectively, with a four mV impedance amplitude, while the cycle stability test was conducted using cyclic charge-discharge measurement. The importance of specific capacitance C_s was determined from Eqs. (1) and (2) to correlate these electrode materials' capacitance performance quantitatively [26].

$$C_{cell} = \frac{1}{mv(V_c - V_a)} \int_{V_a}^{V_c} I(V)dV \quad (1)$$

$$C_s = 4C_{cell} \quad (2)$$

where C_{cell} defines the coin cell's specific capacitance (Fg⁻¹), m signifies the total weight of the two electrodes (g), v denotes the scan rate (mV s⁻¹), $(V_c - V_a)$ the potential sweep range (V), and $I(V)$ the response current (A). Eqs. (3) and (4) were used to compute the energy density, E (Wh kg⁻¹), and power density, P (W kg⁻¹), from the GCD test [27].

$$E = \frac{1}{2} \frac{C_s V^2}{3.6} \quad (3)$$

$$P = \frac{3600 E}{t_d} \quad (4)$$

Respectively, the t_d and V are discharge time (sec) and operating potential (V).

3. Result and discussions

3.1. Morphology and structure characterization

The SEM analysis results of ACO and N-ACU are shown in Fig. 1. Fig. 1a is an SEM image for the ACO sample showing the structure of the interconnected porous network with wrinkles. The effect of variations in the urea doping ratio on morphology demonstrated in Fig. 1b–d shows that the pore structure of the modified activated carbon was formed with interconnected pore clusters [28]. The sample has an irregular granular morphology with abundant pores on the surface [22].

Meanwhile, the morphology, specifically the presence of cavities, is essential concerning energy storage. A previous study confirmed that the pore facilitates electrolyte ion storage [29]. The production of several rough porosities above the sample surface is closely related to the decomposition of the lignocellulosic precursor at elevated temperatures, which causes volatile chemicals to evaporate, leaving freshly created pores [30].

Fig. 2a shows XRD results of pristine and nitrogenated activated carbon samples at the variation of doping ratio. All samples have a broad peak, namely 002 on their XRD curves at 2θ by 26° and a weak band of 100 at 2θ by 43°. This diffraction plane belongs to hexagonal graphite according to JCPDS card no. 41-1487 [31]. The broad peak (002) shows the characteristics of amorphous carbon caused by the activation process, and the presence of a cliff at 100 indicates that the sample contains graphitic carbon [32]. Moreover, the percentage crystallinity values for products N-ACU1, N-ACU2, and N-ACU3 were 19.5, 21.7, and 24.7%, respectively. This value indicates that the more doping compounds are added, the higher the percentage of crystallinity.

Fig. 2b shows the Raman shift of pristine and nitrogenated activated carbon samples at a variation of doping ratio. Two significant peaks were found for activated carbon, centered at about 1590 for graphitic, G,

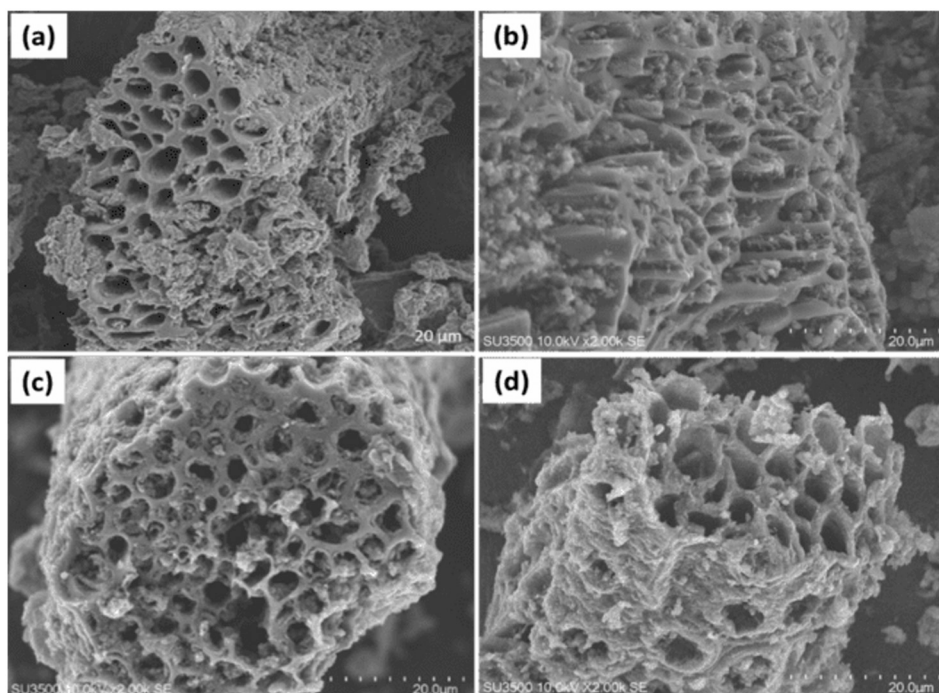


Fig. 1. SEM images of the (a) ACO, (b) N-ACU1, (c) N-ACU2, and (d) N-ACU3.

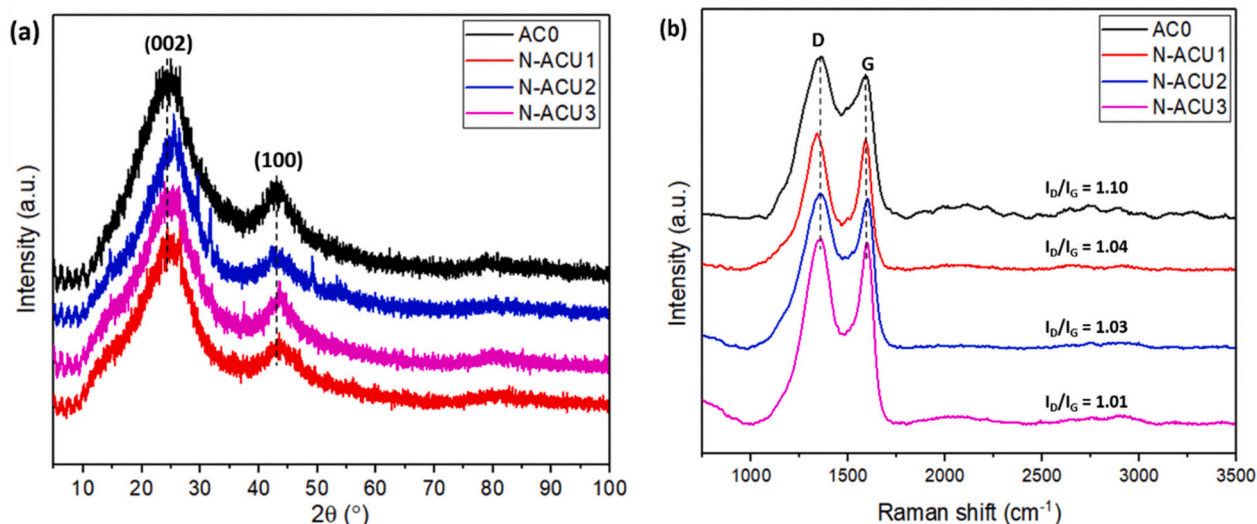


Fig. 2. (a) XRD patterns and (b) Raman spectrums of all as-prepared carbon materials.

and 1341 cm^{-1} for the disordered D band, suggesting an idealized and irregular graphite lattice. The D band, also known as the disruption band, comes from the sp^3 hybridized carbon at the graphene's edge and depicts the severity of the graphite structural flaw. The sp^2 hybridized carbons emerging from the C—C bond strain on the graphitic plane were represented with the G band. The D and G band ratios explain the number of structural flaws in heteroatoms linked to sp^3 carbon [33]. In general, the addition of monoatomic or heteroatomic doping in the manufacture of activated carbon from biomass increases the effect of defects. The intensity of the D peak increases as the number of defects rises, while that of the G peak decreases, which in turn reduces the degree of graphitization [34]. The defect effect produced greater porosity, but Fig. 2b shows that the addition of monoatomic doping did not provide higher defects than the undoped activated carbon. Activated carbon without doping had the highest I_D/I_G ratio with a value of 1.10. With the addition of doping material, there was a slight change in the structure of activated carbon with a decreased I_D/I_G ratio value. For increasing the doping ratio, each I_D/I_G ratio value was 1.01, 1.037, and 1.04. The Raman analysis indicated that the smallest number of structural defects, some of which are from adding atoms for OPEFB activated carbon, was produced from ratio doping of 3 [12].

EDS analysis was applied to quantify the elements contained in activated carbon. The results presented in Fig. 3a show that the ratio of

urea to hydrochar positively affects the content of nitrogen atoms in activated carbon; the greater the ratio, the higher the nitrogen atom content. The impact of ratio doping on the functional groups in the nitrogenated activated carbon surface was analyzed by FTIR spectrometry in the band range of $4500\text{--}400\text{ cm}^{-1}$, as shown in Fig. 3b. The O—H bond's stretching vibration caused the absorption band at 3450 cm^{-1} [35]. Furthermore, the peaks represent CH bond strain vibrations at 2935 cm^{-1} and 2860 cm^{-1} , while the band at 2372 cm^{-1} shows an O=C=O bond, the spectra at 1583 cm^{-1} indicate a C=C bond, and spectra at 1463 cm^{-1} is defined as a CN asymmetric stretching vibration. The bands formed at $1072\text{--}1141.9\text{ cm}^{-1}$ indicate the C—O bonds, including primary alcohols, and esters, while the absorption band of 950.5 cm^{-1} depicts the =C—H bond [36].

The activated carbon porosity studies were performed based on nitrogen's physical adsorption. Porosity can generally be classified based on pore size and accessibility, namely open or closed. The N_2 isotherms of adsorption and desorption curves for each of the doped activated carbon products are shown in Fig. 4. According to the International Union of Pure and Applied Chemistry's (IUPAC) definition, a type-IV isotherm was found in every sample, with a pronounced loop of hysteresis in the range $0.10\text{--}0.99\text{ P/P}_0$ indicating a mesoporous structure [37]. The volume of N_2 adsorbed at P/P_0 , namely 0.97 experienced a significant increase, specifically for the 1 and 2 doping ratios, indicating

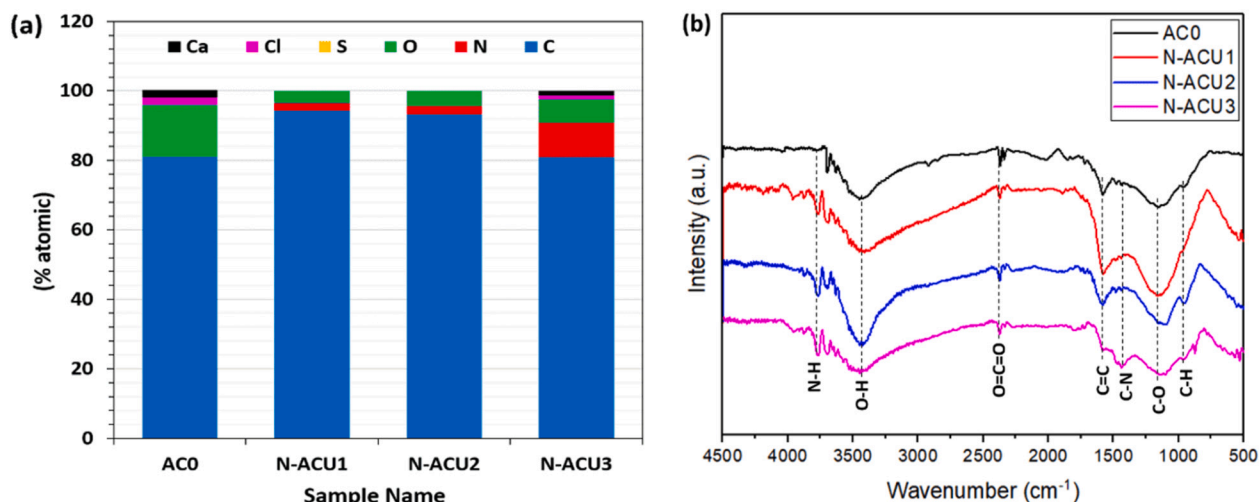


Fig. 3. (a) SEM-EDS analysis of atomic and (b) IR spectra of all as-prepared carbon materials.

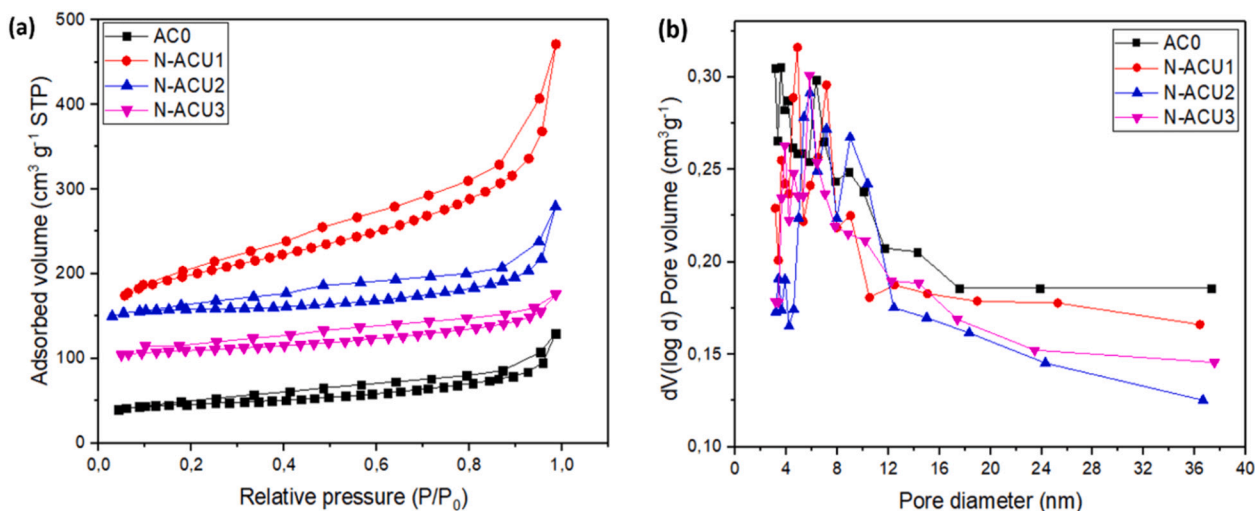


Fig. 4. (a) Nitrogen adsorption/desorption isotherm and (b) pore size distribution of all sample.

the existence of large voids and/or mesopores. Fig. 4a shows that the volume adsorbed gradually reduced with increasing doping ratio. The pore size distribution map in Fig. 4b confirms the mesoporous nature of activated carbon, which displays samples with pore diameters ranging from 3.3 to 38 nm. The four samples in Fig. 4b had a pore size distribution with narrow peaks between 3.6 and 5 nm, affirming the doping ratio's effect on the pore structure [38].

The surface area of BET (S_{BET}) and the porosity characteristics of the activated carbon products are shown in Table 1.

According to Liu et al. [6], the mechanism of forming the porous structure of nitrogenated activated carbon from biomass with a CaCl_2 activator is related to several factors. During heat treatment in the hydrothermal carbonization process, CaCl_2 had a significant water removal effect on the cellulose, hemicellulose, and lignin components. This is because CaCl_2 species can seep into the framework of the biomass structure. Subsequently, the main crystal structure was changed, with CaCl_2 enhancing its wide dispersion into the biomass framework. Urea was added to the hydrochar impregnation stage to serve as a nitrogen developer. Meanwhile, NH_3 produced by in situ breakdowns of ammonia precursors such as urea combines with the carbon and widely dispersed CaCl_2 aggregates to generate $\text{CaCl}_2 \cdot 2\text{H}_2\text{O}$ crystals (JCPDS: 70-0385) during the activation step at high temperatures.

The activation process involves the coexistence of interconnected macropores, micro, and mesopores which porosity develops into the structure. Also, it contains nitrogen functional groups which can be incorporated into the framework. Porous nitrogen-doped carbon tends to have graphitization, high specific surface area, and unique morphology. After washing with water and HCl, the reaction with Ca^{2+} and dissolved carbonates produced the compound CaCl_2 and a minor quantity of CaCO_3 , leading to a porous structure of nitrogen-rich carbon [1,13]. The porous properties of synthesized activated carbon were compared to values reported in the literature for various activated carbons, as shown in Table 2.

In general, the characteristic of biomass-based-activated carbon is highly influenced by raw material properties (such as fixed carbon,

Table 1
Characteristics of the pore structure of activated carbon sample.

No	Sample	S_{BET} ($\text{m}^2 \text{g}^{-1}$)	D_a (nm)	V_t ($\text{cm}^3 \text{g}^{-1}$)
1	AC0	363,88	3,30	0,22
2	N-ACU1	640,61	3,09	0,73
3	N-ACU2	477,51	5,80	0,43
4	N-ACU3	445,18	3,80	0,30

D_a : pore diameter, V_t : total pore volume.

Table 2
Comparison of the surface area of activated carbon synthesized from different biomass.

Carbon precursor	Activating agent	S_{BET} ($\text{m}^2 \text{g}^{-1}$)	V_{total} ($\text{cm}^3 \text{g}^{-1}$)	D_p (nm)	References
Pomelo mesocarps	CaCl_2	974.6	0.69	2.9	[1]
Sugar cane bagasse	CaCl_2	805.5	0.68	3.38	[6]
Oil palm empty fruits bunch	KOH	1704	0.89	2.24	[18]
Oil palm empty fruits bunch	ZnCl_2	1571	–	2.13	[20]
Tobacco stalk	KOH	3177	–	–	[39]
Rotten carrot	ZnCl_2	1155	0.93	3.2	[40]
Pea skin	ZnCl_2	1253	0.95	3.1	[41]
N doped pea skin	KOH	1828	0.97	2.1	[42]
Butnea monosperma	ZnCl_2	1422	0.77	2.2	[43]
Cocoa shell	ZnCl_2	619	0.32	4.8	[44]
Rice husk	H_3PO_4	298	1.19	2.5	[45]
Rice husk	H_3PO_4	1493	1.21	3.25	[46]
Cotton stalk	KOH	1964	1.03	0.88	[47]
Sago waste	ZnCl_2	546.6	0.30	3.3	[48]
Rubberwood sawdust	–	912	0.61	2.6	[49]
Firewood	K_2CO_3	818	0.44	2.1	[50]
N modified oil palm empty-fruits bunch	CaCl_2	640.6	0.73	3.09	This work

volatile matter, moisture, and ash content), activating agent type, carbonization time, impregnation ratio, and carbonization temperature. In other words, the different source materials and activation procedures can produce activated carbons with a wide range of properties. Activated carbon from the same raw material but synthesized with different activating agents will produce other surface areas. Activated carbon with the activating agent CaCl_2 has a lower surface area than KOH and ZnCl_2 because of the differences in its dehydrating and oxidizing effect and molecular sizes. However, CaCl_2 is cheaper than ZnCl_2 . The efficiency of activation and the cost should be considered in approaches to a practical activation process [51].

3.2. Electrochemical properties

The electrochemical performance of all samples was assessed in a two-electrode system. CV analysis aims to determine the characteristics of the cell and the value of the specific capacitance of supercapacitors.

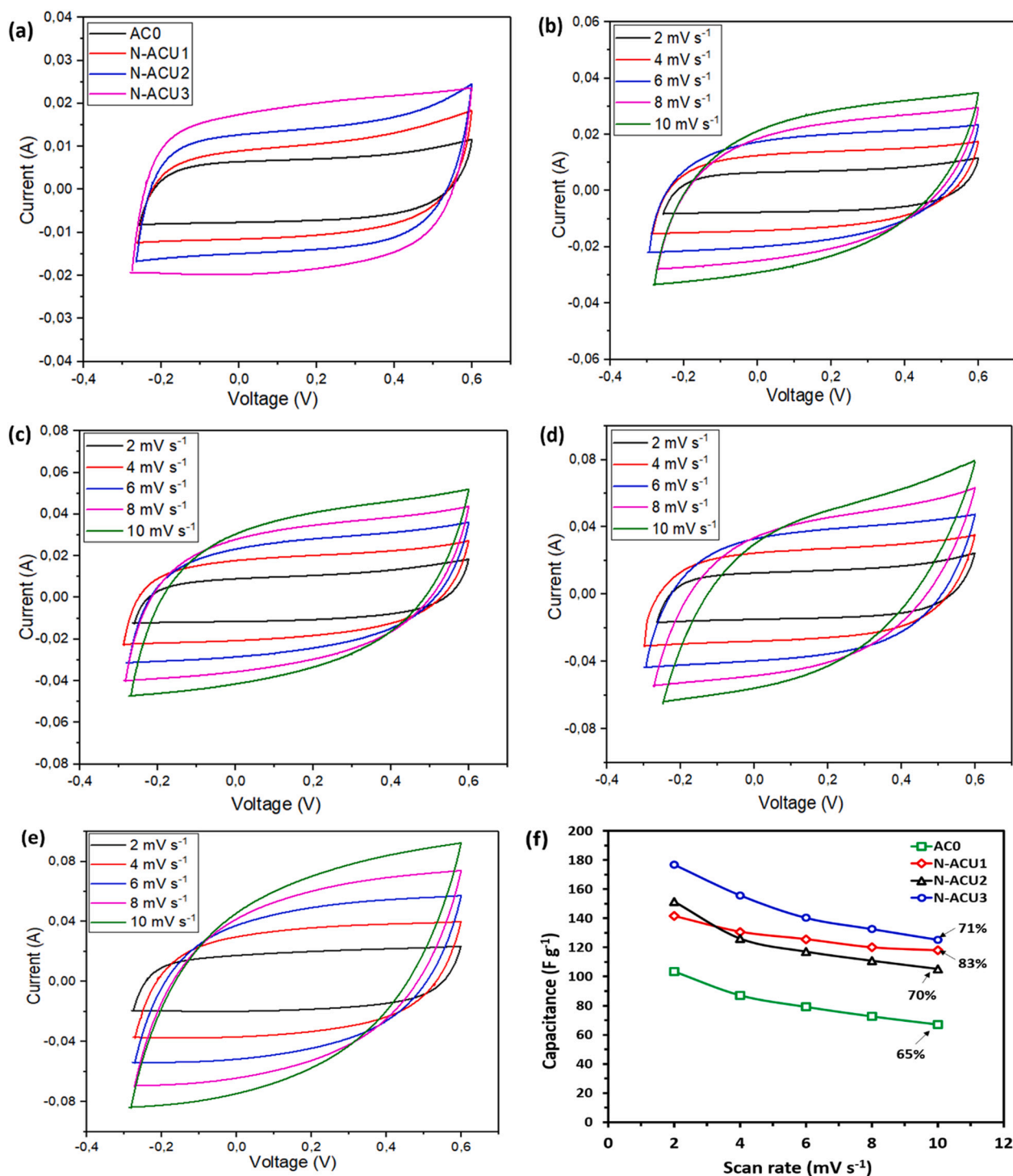


Fig. 5. CV curve of supercapacitor cells (a) all samples at 2 mV s^{-1} , (b) AC0, (c) N-ACU1, (d) N-ACU2, (e) N-ACU3, and (f) the rate capability of all sample.

Fig. 5a shows the CV analysis for supercapacitors of modified urea doped activated carbon (N-ACU) and non-doped activated carbon (AC0) at a scan rate of 2 mV s^{-1} . The shape of the voltammogram curve for sample N-ACU3 has an ideal quasi-rectangle shape without redox peaks.

The excellent rectangular shape of the cyclic voltammogram shows that the primary electricity and double layer capacitance are formed because several ions were adsorbed on the electrode's surface with the electrolyte's diffusion limit. Moreover, the sample curves for N-ACU1 and N-ACU2 are quasi-rectangle with peaks at the right end edge, indicating the redox effect caused by the nitrogen functional group. The

AC0 sample tends to be oblique parallelogram indicating a fast charging and discharging process with low series resistance and significant power supply capability [52]. The N-ACU3 curve shows the largest closed area among all samples, indicating the highest capacitance. Fig. 5b–e shows the CV curve at 2–10 mV s^{-1} for AC0, N-ACU1, N-ACU2, and N-ACU3, respectively.

The higher the scan rate, the greater the parallelograms nature of the cyclic voltammogram curves for all supercapacitor cells without redox peaks, indicating the absence of pseudocapacitive phenomena and good performance [53]. Fig. 5f shows that the higher the scan rate, the lower

the specific capacitance value. At low scan rates, the cyclic voltammogram offers ideal capacitive behavior. However, as the scan rate increases, this perfect behavior is distorted with a gradual decrease in capacitance. This is prevalent in activated carbon materials when a drop in specific capacitance occurs due to insufficient time for ion transport and adsorption within the tiniest pores in big particles. Decreasing capacitance is due to obstacles to the transfer of ions from the electrolyte to the electrode surface; hence, all electrode pores cannot be accessed at high scan rates [53]. Fig. 5f shows that among the several supercapacitor cells based on ordinary and modified activated carbon, N-ACU2 cells have the highest capability rate, namely 83%. The high specific surface area, N-doping, and rich mesoporous structure contribute to the high rate capability. Besides, the high specific surface area and the tremendous mesoporous system can facilitate even more active sites for ion adsorption.

Nitrogen enrichment can upgrade the electrode material's wettability and hydrophilicity and promote ion transport [52]. According to Yuan et al., N doping significantly increased the supercapacitor-specific capacitance of activated carbon synthesized from biomass, specifically tobacco stems but decreased rate capability and cycle stability. Excessive doping damages the material's structure because it causes a more disordered system affecting electron transport efficiency [39].

The GCD curve shows the voltage response of the tested supercapacitor cells at a constant current. Cell voltage was measured as a charge and discharge time [38], while GCD analysis for each supercapacitor cell was carried out at consistent current densities of 1, 2, 3, 4,

and 4 A g⁻¹; the curve for all samples presented in Fig. 6 shows a symmetrical triangular shape with a low voltage drop. This type of curve is characteristic of carbon-based supercapacitor cells [18].

The voltage drop indicates a less than ideal charge/discharge process, showing that the ions are not entirely desorbed at a given current value. The electrolyte ions react with the electrodes, leading to equivalent series resistance. A previous study reported that a low voltage drop indicates that the supercapacitor cell has good power characteristics [13]. The GCD curve can be used as a parameter to determine the operating voltage, namely the appropriate working voltage for supercapacitor cells to operate safely [12]. Based on Fig. 6, the safe voltage for a supercapacitor cell is 0.9–1.0 V for a single cell.

Energy and power densities were quantified by Eqs. (3) and (4), and the results are presented in Table 2, which shows the highest energy density of 19.89 Wh kg⁻¹ for N-ACU3 and 8.08 Wh kg⁻¹ for ACO. Meanwhile, the highest power density was 1431.20 W kg⁻¹ for the N-ACU3 sample, and the lowest was 484.83 W kg⁻¹ for ACO. These values show that the modification of activated carbon with N doping increases the energy density and power due to the redox effect and the enhancement in the conductivity of the nitrogenated activated carbon [54] (Table 3).

EIS was performed to characterize the electrochemical properties of the supercapacitor, including the electrolyte/electrode interface and diffuse resistance; the curve obtained was represented in the Nyquist plot. The Nyquist plot of an ideal supercapacitor cell consists of a semicircle at high frequencies, followed by a slash (45°) at medium

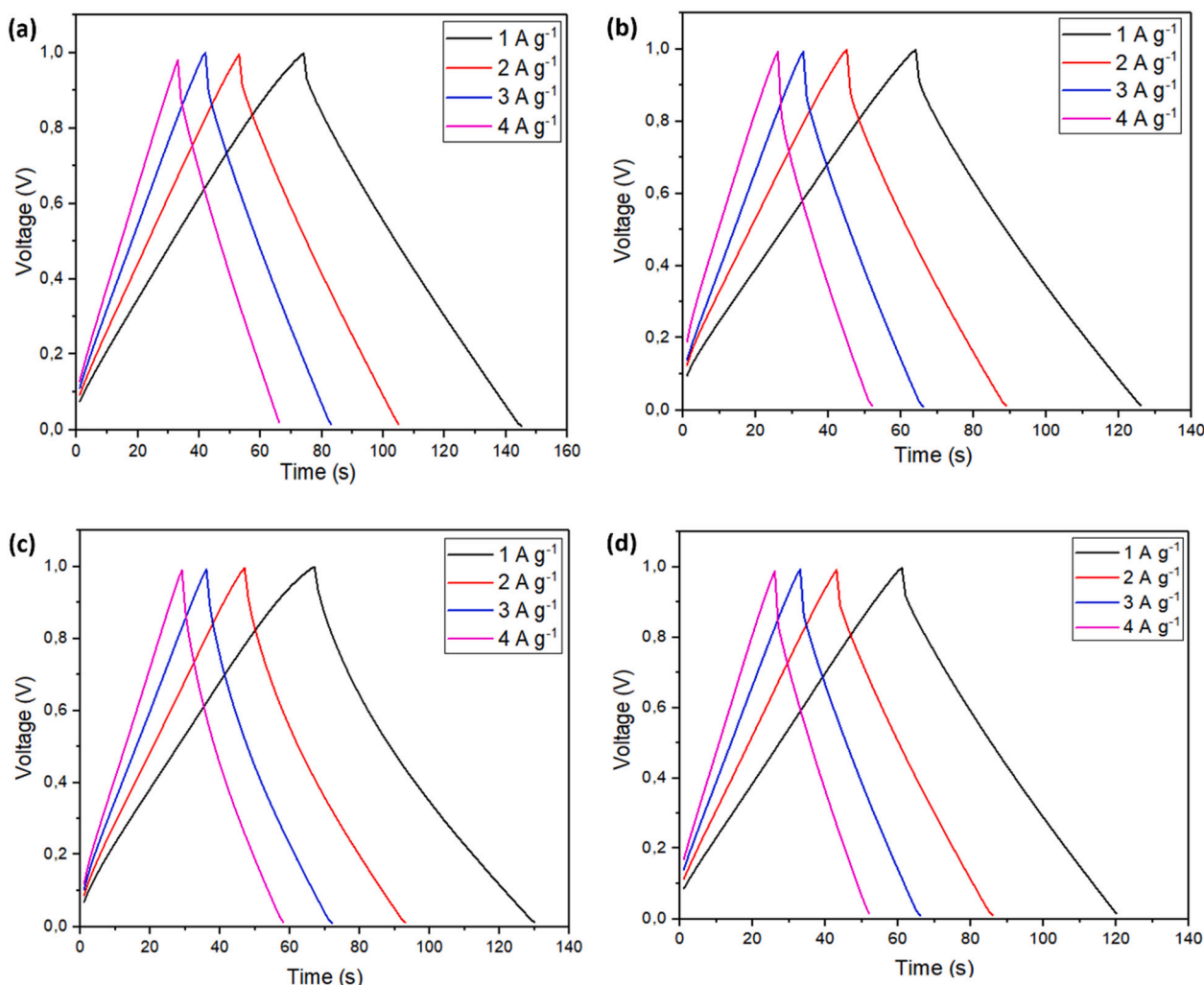


Fig. 6. GCD curve of supercapacitor cells (a) ACO, (b) N-ACU1, (c) N-ACU2, and (d) N-ACU3.

Table 3
The performance of activated carbon-based supercapacitor.

No	Sample	C_s ($F g^{-1}$)	E ($Wh kg^{-1}$)	P ($W kg^{-1}$)
1	AC0	103.43	8.08	484.83
2	N-ACU1	141.47	11.05	795.77
3	N-ACU2	151.60	13.48	970.24
4	N-ACU3	176.76	19.89	1431.20

frequencies and a perpendicular (90°) at low frequencies. The starting point in the semicircle represents the electrolyte resistance (R_s), while the semicircle shape represents the cell impedance affected by charge transfer resistance (R_{ct}). At medium to low frequencies, there is opposition to ion transfer into the pores of the electrode (R_w) [55]. EIS curves for all experimental samples are presented in Fig. 7a, showing that increasing the doping ratio affects electrolyte resistance. The greater the doping ratio, the smaller the electrolyte resistance at high frequency. Some samples showed fully and partially formed semicircular loops at medium-high frequencies. The smaller the semicircle, the lower the charge transfer resistance at the electrolyte/electrode interface [56] due to the N content. Furthermore, the N content influences the wettability of the electrode on the electrolyte and increases the conductivity. Electrolyte and small charge transfer resistance are essential in expanding the supercapacitor rate capability [32].

As shown in Fig. 7a, the electrolyte resistance in order was N-ACU3 < N-ACU2 < N-ACU1 < AC0, while the R_s values of each sample were 0.40, 0.55, 0.80, and 1.3 Ω . Furthermore, the R_{ct} values of each sample from semicircle shape in order N-ACU2 < N-ACU3 < N-ACU1 < AC0 were 0.5, 0.8, 0.85, and 1.1 Ω , while the R_w values were 0.3, 0.5, 0.4, and 0.5 Ω for N-ACU3, N-ACU2, N-ACU1, and AC0, respectively. The EIS curve shows that the modification of activated carbon with nitrogen doping can reduce electrolyte resistance and charge transfer. However, the pore mass transfer resistance was relatively similar because the pore

sizes of ordinary and nitrogenated activated carbon were in the same mesoporous range.

The supercapacitor durability and cyclic stability test were carried out using a potentiostat by cyclic charge-discharge (CCD) measurement. The charge/discharge character of the supercapacitor in the multicycle was obtained at a particular voltage and current for the specific cycle. Moreover, the life cycle of the supercapacitor was determined by considering the value of coulombic efficiency (CE) and retention capacitance (CR). CE is the discharge-to-charge capacity ratio in the current cycle [39], while CR is the ratio between the capacitance of each process with the initial capacitance. The CE values for AC0 and N-ACU3-based-supercapacitor were stable at 94% and 100%, respectively, while the CR values remained at 81% and 98.7%, respectively, for 5000 cycles. Fig. 7b shows that activated carbon modification with N doping did not decrease the cell cycle stability at constant voltage and working current values but had an excellent capacitive performance. A high CE also indicates that the potential for side reactions at the electrode surface is minimum [33]. The Ragone plot from Fig. 7c depicted the symmetric supercapacitor's energy density and power density. These findings suggest that activated carbon with a nitrogenated mesopore structure and an organized pore structure could increase energy density.

Table 4 shows the comparative properties of several supercapacitor topologies using biomass-activated carbon-based electrodes. Compared with the previously reported electrode materials in Table 4, the capacitance value of this study is quite good and higher than the reference [18], which indicates that nitrogen modification of biomass is a promising method for upgrading the supercapacitor performance.

4. Conclusions

The nitrogenated mesoporous activated carbon (N-ACU) was successfully produced from empty fruit bunches of oil palm by hydrothermal carbonization and CO_2 gas activation. Porosity analysis showed that

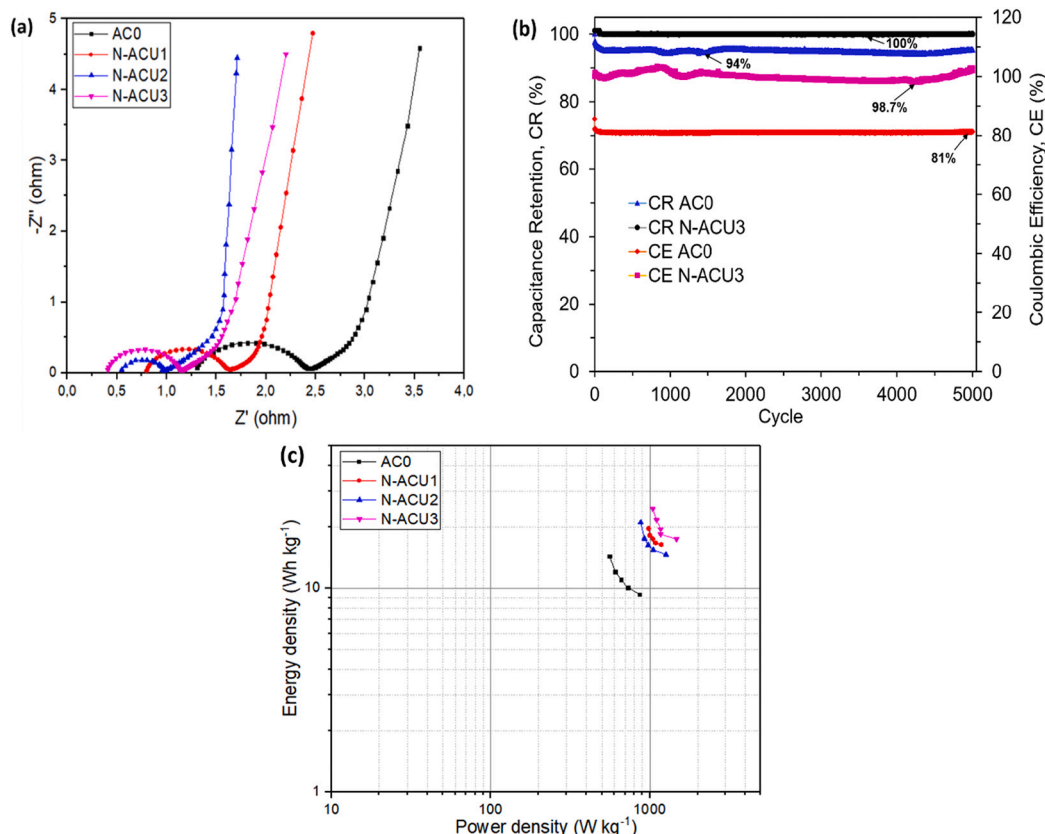


Fig. 7. (a) Nyquist plot of all samples, (b) cyclic stability of AC0 and N-ACU3 based-cell, (c) Ragone plot for all of the supercapacitor cells.

Table 4

The electrochemical parameters of activated carbon electrodes from different biomass/biowaste.

Biomass	Electrolyte	C_s (F g^{-1}) ^a	E (Wh kg^{-1})/P (W kg^{-1})	Stability ^b (%) / Cycle	References
Pomelo mesocarps	2 M KOH	245 (0.5 A g^{-1})	14.7/90		[1]
Oil palm empty fruits bunch	1 M H ₂ SO ₄	150 (10 mA cm^{-2})	4.3/173.3	–	[18]
N modified-coconut shell	6 M KOH	179 (0.5 A g^{-1})	–	84/2500	[35]
Tobacco stalk	6 M KOH	281 (1 A g^{-1})	6.51/3000	78/10000	[39]
Rotten carrot	1 M LiClO ₄	142.7 (1 mA cm^{-2})	28.4/89,100		[40]
Pea skin	1 M H ₂ SO ₄	192.7 (1 mA cm^{-2})	7.5/1700	85/5000	[41]
N doped-pea skin	1 M LiTFSI	141.1 (1.3 A g^{-1})	19.60/25,400	75/5000	[42]
Butnea monosperma	6 M KOH	130.5 (1 mA cm^{-2})	4.53/2070	99/10000	[43]
Rice husk	1 M H ₂ SO ₄	112 (1 A g^{-1})	15.5/1421	–	[46]
Rubberwood sawdust	1 M H ₂ SO ₄	138 (1 A g^{-1})	2.63/291	–	[49]
Firewood	1 M H ₂ SO ₄	189 (0.2 A g^{-1})	–	85/5000	[50]
Nettle leaves	EMIM BF ₄	163 (0.5 A g^{-1})	50/372	92/10000	[57]
N modified-oil palm empty fruits bunch	6 M KOH	176.7 (2 mV s^{-1})	19.8/1431.2	98/5000	This work

^a Specific capacitance at current density or scan rate.

^b As capacitance retention.

all samples had a mesoporous structure ranging from 3.3–5.8 nm and a BET surface area of 363.88–640.61 $m^2 g^{-1}$. At the same time, the electrochemical characterization indicated that the ratio of urea to hydrochar impregnation affects the performance of the supercapacitor. Furthermore, electrode-specific capacitance values for all samples were 103.43, 141.47, 151.60, and 176.76 $F g^{-1}$ at 2 $mV s^{-1}$ for AC0, N-ACU1, N-ACU2, and N-ACU3. In contrast, the best energy and power density values at the current 1 $A g^{-1}$ were 19.89 $Wh kg^{-1}$ and 1431.20 $W kg^{-1}$, respectively, for the N-ACU3 sample. Durability tests conducted for N-ACU3 supercapacitor by cyclic charge-discharge for 5000 cycles showed that the coulombic efficiency and capacitance retention were close to 100% and 98.7%, respectively. Based on the results, the urea to hydrochar impregnation ratio affects the characteristic of N-ACU and the performance of supercapacitors. Urea nitrogenated treatment on activated carbon can reduce the ohmic and charge transfer resistance and maintain the supercapacitor's cell stability. The improved supercapacitor performance indicates that the synthesis of nitrogenated activated carbon from biomass waste can be a promising method for producing electrode materials.

CRediT authorship contribution statement

Heri Rustamaji: Methodology, Data curation, Investigation, Formal analysis, Writing – original draft. **Tirto Prakoso:** Conceptualization, Writing – review & editing, Supervision. **Hary Devianto:**

Conceptualization, Writing – review & editing, Supervision. **Pramujo Widiatmoko:** Writing – review & editing. **Wibawa Hendra Saputera:** Conceptualization, Supervision.

Declaration of competing interest

The authors declare that they have no known competing financial interests or personal relationships that could have appeared to influence the work reported in this paper.

Acknowledgment

The author is grateful to the Indonesia Endowment Fund for Education or LPDP (Lembaga Pengelola Dana Pendidikan) through schema BUDI-DN (No. 2020022102189) for funding this research.

References

- [1] H. Peng, G. Ma, K. Sun, Z. Zhang, Q. Yang, Z. Lei, Nitrogen-doped interconnected carbon nanosheets from pomelo mesocarps for high-performance supercapacitors, *Electrochim. Acta* 190 (2016) 862–871, <https://doi.org/10.1016/j.electacta.2015.12.195>.
- [2] C. Wang, D. Wu, H. Wang, Z. Gao, F. Xu, K. Jiang, Biomass-derived nitrogen-doped hierarchical porous carbon sheets for supercapacitors with high performance, *J. Colloid Interface Sci.* 523 (2018) 133–143, <https://doi.org/10.1016/j.jcis.2018.03.009>.
- [3] B.K. Kim, S. Sy, A. Yu, J. Zhang, Electrochemical supercapacitors for energy storage and conversion, in: *Handb. Clean Energy Syst.*, 2015, pp. 1–25, <https://doi.org/10.1002/9781118991978.hces112>.
- [4] Y. Hu, H. Liu, Q. Ke, J. Wang, Effects of nitrogen doping on supercapacitor performance of a mesoporous carbon electrode produced by a hydrothermal soft-templating process, *J. Mater. Chem. A* 2 (30) (2014) 11753–11758, <https://doi.org/10.1039/c4ta01269k>.
- [5] P. Simon, Y. Gogotsi, Perspectives for electrochemical capacitors and related devices, *Nat. Mater.* 19 (11) (2020) 1151–1163, <https://doi.org/10.1038/s41563-020-0747-z>.
- [6] J. Liu, Y. Deng, X. Li, L. Wang, Promising nitrogen-rich porous carbons derived from one-step calcium chloride activation of biomass-based waste for high-performance supercapacitors, *ACS Sustain. Chem. Eng.* 4 (1) (2016) 177–187, <https://doi.org/10.1021/acsschemeng.5b00926>.
- [7] M. Biswal, A. Banerjee, M. Deo, S. Ogale, From dead leaves to high energy density supercapacitors, *Energy Environ. Sci.* 6 (4) (2013) 1249–1259, <https://doi.org/10.1039/c3ee22325f>.
- [8] W. Raza, et al., Recent advancements in supercapacitor technology, *Nano Energy* 52 (August) (2018) 441–473, <https://doi.org/10.1016/j.nanoen.2018.08.013>.
- [9] J. Jiang, Y. Li, J. Liu, X. Huang, C. Yuan, X.W. Lou, Recent advances in metal oxide-based electrode architecture design for electrochemical energy storage, *Adv. Mater.* 24 (38) (2012) 5166–5180, <https://doi.org/10.1002/adma.201202146>.
- [10] R. Ramya, R. Sivasubramanian, M.V. Sangaranarayanan, Conducting polymer-based electrochemical supercapacitors - progress and prospects, *Electrochim. Acta* 101 (2013) 109–129, <https://doi.org/10.1016/j.electacta.2012.09.116>.
- [11] A. Gopalakrishnan, S. Badhulika, Effect of self-doped heteroatoms on the performance of biomass-derived carbon for supercapacitor applications, *J. Power Sources* 480 (June) (2020), 228830, <https://doi.org/10.1016/j.jpowsour.2020.228830>.
- [12] K. Dujearic-Stephane, The effect of modifications of activated carbon materials on the capacitive performance: surface, microstructure, and wettability, *J. Compos. Sci.* 5 (3) (2021), <https://doi.org/10.3390/jcs5030066>.
- [13] B. Li, et al., Nitrogen-doped activated carbon for a high energy hybrid supercapacitor, *Energy Environ. Sci.* 9 (1) (2016) 102–106, <https://doi.org/10.1039/c5ee03149d>.
- [14] F. Gao, G. Shao, J. Qu, S. Lv, Y. Li, M. Wu, Tailoring of porous and nitrogen-rich carbons derived from hydrochar for high-performance supercapacitor electrodes, *Electrochim. Acta* 155 (2015) 201–208, <https://doi.org/10.1016/j.electacta.2014.12.069>.
- [15] M. Wu, P. Li, Y. Li, J. Liu, Y. Wang, Enteromorpha based porous carbons activated by zinc chloride for supercapacitors with high capacity retention, *RSC Adv.* 5 (21) (2015) 16575–16581, <https://doi.org/10.1039/c4ra13428a>.
- [16] D. Perkebunan, Statistik Perkebunan Indonesia (tree crop estate statistics of Indonesia 2017–2019) Kelapa Sawit (Palm Oil) [Online]. Available, in: Dir. Gen. Estate Crop. Minist. Agric. Indones, 2018, pp. 1–81 <http://ditjenbun.pertanian.go.id>.
- [17] A. Thambidurai, J.K. Lourdasamy, J.V. John, S. Ganesan, Preparation and electrochemical behavior of biomass-based porous carbons as electrodes for supercapacitors - a comparative investigation, *Korean J. Chem. Eng.* 31 (2) (2014) 268–275, <https://doi.org/10.1007/s11814-013-0228-z>.
- [18] R. Farma, et al., Preparation of highly porous binderless activated carbon electrodes from fibers of oil palm empty fruit bunches for application in supercapacitors, *Bioresour. Technol.* 132 (2013) 254–261, <https://doi.org/10.1016/j.biortech.2013.01.044>.

- [19] R. Hendriansyah, T. Prakoso, P. Widiatmoko, I. Nurdin, H. Devianto, Manufacturing carbon material by carbonization of cellulosic palm oil waste for supercapacitor material, *MATEC Web Conf.* 156 (2018), <https://doi.org/10.1051/mateconf/201815603018>.
- [20] T.D. Larasati, T. Prakoso, J. Rizkiana, H. Devianto, P. Widiatmoko, I. Nurdin, Nano carbon produced by advanced mild hydrothermal process of oil palm biomass for supercapacitor material, *IOP Conf. Ser. Mater. Sci. Eng.* 543 (1) (2019), <https://doi.org/10.1088/1757-899X/543/1/012031>.
- [21] N.N. Wulandari, et al., Production of activated carbon from palm empty fruit bunch as supercapacitor electrode material, *IOP Conf. Ser. Mater. Sci. Eng.* 1143 (1) (2021), 012004, <https://doi.org/10.1088/1757-899X/1143/1/012004>.
- [22] Y. Zhu, M. Chen, Y. Zhang, W. Zhao, C. Wang, A biomass-derived nitrogen-doped porous carbon for high-energy supercapacitor, *Carbon N. Y.* 140 (2018) 404–412, <https://doi.org/10.1016/j.carbon.2018.09.009>.
- [23] A. Jain, C. Xu, S. Jayaraman, R. Balasubramanian, J.Y. Lee, M.P. Srinivasan, Mesoporous activated carbons with enhanced porosity by optimal hydrothermal pre-treatment of biomass for supercapacitor applications, *Microporous Mesoporous Mater.* 218 (2015) 55–61, <https://doi.org/10.1016/j.micromeso.2015.06.041>.
- [24] J. Wu, Z. Pan, Y. Zhang, B. Wang, H. Peng, The recent progress of nitrogen-doped carbon nanomaterials for electrochemical batteries, *J. Mater. Chem. A* 6 (27) (2018) 12932–12944, <https://doi.org/10.1039/c8ta03968b>.
- [25] V. da Silva Lacerda, et al., Rhodamine B removal with activated carbons obtained from lignocellulosic waste, *J. Environ. Manag.* 155 (2015) 67–76, <https://doi.org/10.1016/j.jenvman.2015.03.007>.
- [26] H. Cao, X. Peng, M. Zhao, P. Liu, B. Xu, J. Guo, Oxygen functional groups improve the energy storage performances of graphene electrochemical supercapacitors, *RSC Adv.* 8 (6) (2018) 2858–2865, <https://doi.org/10.1039/c7ra12425b>.
- [27] J. Zhou, et al., Porous carbon materials with dual N, S-doping and uniform ultramicroporosity for high-performance supercapacitors, *Electrochim. Acta* 209 (2016) 557–564, <https://doi.org/10.1016/j.electacta.2016.05.127>.
- [28] K. Chaitra, et al., KOH activated carbon derived from biomass-banana fibers as an efficient negative electrode in a high-performance asymmetric supercapacitor, *J. Energy Chem.* 26 (1) (2017) 56–62, <https://doi.org/10.1016/j.jechem.2016.07.003>.
- [29] S. Ahmed, M. Rafat, A. Ahmed, Nitrogen-doped activated carbon derived from orange peel for supercapacitor application, *Adv. Nat. Sci. Nanosci. Nanotechnol.* 9 (3) (2018), <https://doi.org/10.1088/2043-6254/aad5d4>.
- [30] K.R. Thines, E.C. Abdullah, M. Ruthiraan, N.M. Mubarak, M. Tripathi, A new route of magnetic biochar based polyaniline composites for supercapacitor electrode materials, *J. Anal. Appl. Pyrolysis* 121 (2016) 240–257, <https://doi.org/10.1016/j.jaap.2016.08.004>.
- [31] J. Hou, C. Cao, F. Idrees, X. Ma, Hierarchical porous nitrogen-doped carbon nanosheets derived from silk for ultrahigh-capacity battery anodes and supercapacitors, *ACS Nano* 9 (3) (2015) 2556–2564, <https://doi.org/10.1021/nl506394r>.
- [32] C. Wang, et al., Ultrahigh yield of nitrogen-doped porous carbon from biomass waste for supercapacitor, *Renew. Energy* 156 (2020) 370–376, <https://doi.org/10.1016/j.renene.2020.04.092>.
- [33] M. Barczak, T.J. Bandosz, Evaluation of nitrogen- and sulfur-doped porous carbon textiles as electrode materials for flexible supercapacitors, *Electrochim. Acta* 305 (2019) 125–136, <https://doi.org/10.1016/j.electacta.2019.03.014>.
- [34] J. Zhou, et al., Nitrogen-doped hierarchically porous carbon materials prepared from meta-aminophenol formaldehyde resin for supercapacitor with high rate performance, *Electrochim. Acta* 153 (2015) 68–75, <https://doi.org/10.1016/j.electacta.2014.11.075>.
- [35] W. Yang, Y. Li, Y. Feng, High electrochemical performance from oxygen functional groups containing porous activated carbon electrode of supercapacitors, *Materials (Basel)* 11 (12) (2018), <https://doi.org/10.3390/ma11122455>.
- [36] M.F. Shabik, H. Begum, M.M. Rahman, H.M. Marwani, M.A. Hasnat, Heterogeneous kinetics of thiourea electro-catalytic oxidation reactions on palladium surface in aqueous medium, *Chem. Asian J.* 15 (24) (2020) 4327–4338, <https://doi.org/10.1002/asia.202001016>.
- [37] Y. Zhang, Y. Zhang, J. Huang, D. Du, W. Xing, Z. Yan, Enhanced capacitive performance of N-doped activated carbon from petroleum coke by combining amoxidation with KOH activation, *Nanoscale Res. Lett.* 11 (1) (2016) 0–6, <https://doi.org/10.1186/s11671-016-1460-3>.
- [38] J. Yu, et al., Tailoring in-situ N, O, P, S-doped soybean-derived porous carbon with ultrahigh capacitance in both acidic and alkaline media, *Renew. Energy* 163 (2021) 375–385, <https://doi.org/10.1016/j.renene.2020.08.066>.
- [39] Q. Yuan, et al., N, S-codoped activated carbon material with ultra-high surface area for high-performance supercapacitors, *Polymers* 12 (9) (2020) 1–14, <https://doi.org/10.3390/polym12091982>.
- [40] S. Ahmed, A. Ahmed, M. Rafat, Supercapacitor performance of activated carbon derived from rotten carrot in aqueous, organic and ionic liquid-based electrolytes, *J. Saudi Chem. Soc.* 22 (2018) 993–1002, <https://doi.org/10.1016/j.jscs.2018.03.002>.
- [41] S. Ahmed, A. Ahmed, M. Rafat, Impact of aqueous and organic electrolytes on the supercapacitive performance of activated carbon derived from pea skin, *Surf. Coat. Technol.* 349 (2018) 242–250, <https://doi.org/10.1016/j.surfcoat.2018.05.073>.
- [42] S. Ahmed, A. Ahmed, M. Rafat, Nitrogen-doped activated carbon from pea skin for high-performance supercapacitor, *Mater. Res. Express* 5 (2018), 045508, <https://doi.org/10.1088/2053-1591/aabbe7>.
- [43] S. Ahmed, A. Ahmed, M. Rafat, Investigation on activated carbon derived from biomass butnea monosperma and its application as a high-performance supercapacitor electrode, *J. Energy Storage* 26 (2019), 100988, <https://doi.org/10.1016/j.est.2019.100988>.
- [44] C. Saucier, M.A. Adebayo, E.C. Lima, R. Cataluna, P.S. Thue, L.D. Prola, M. J. Puchana-Rosero, F.M. Machado, F.A. Pavan, G.L. Dotto, Microwave-assisted activated carbon from the cocoa shell as adsorbent for removal of sodium diclofenac and nimesulide from aqueous effluents, *J. Hazard. Mater.* 289 (2015) 18–27, <https://doi.org/10.1016/j.jhazmat.2015.02.026>.
- [45] S. Somasundaram, K. Sekar, V.K. Gupta, S. Ganesan, Synthesis and characterization of mesoporous activated carbon from rice husk for adsorption of glycine from the alcohol-aqueous mixture, *J. Mol. Liq.* 177 (2013) 416–425, <https://doi.org/10.1016/j.molliq.2012.09.022>.
- [46] A. Ganesan, R. Mukherjee, J. Raj, M.M. Shaijumon, Nanoporous rice husk derived carbon for gas storage and high-performance electrochemical energy storage, *J. Porous Mater.* 21 (2014) 839–847, <https://doi.org/10.1007/s10934-014-9833-4>.
- [47] X. Tian, H. Ma, Z. Li, S. Yan, L. Ma, F. Yu, G. Wang, X. Guo, Y. Ma, C. Wong, Flute type micropores activated carbon from cotton stalk for high-performance supercapacitors, *J. Power Sources* 359 (2017) 88–96, <https://doi.org/10.1016/j.jpowsour.2017.05.054>.
- [48] O. Togibasa, M. Mumfajjah, Y.K. Allo, K. Dahlan, Y.O. Ansanay, The effect of the chemical activating agent on the properties of activated carbon from sago waste, *Appl. Sci.* 11 (2021) 11640, <https://doi.org/10.3390/app112411640>.
- [49] E. Taer, M. Deraman, I.A. Talib, A. Awitdrus, S.A. Hashmi, A.A. Umar, Preparation of a highly porous binderless activated carbon monolith from rubberwood sawdust by a multi-step activation process for application in supercapacitors, *Int. J. Electrochem. Sci.* 6 (2011) 3301–3315.
- [50] B. Lu, L. Hu, H. Yin, W. Xiao, D. Wang, One-step molten salt carbonization (MSC) of firewood biomass for capacitive carbon, *RSC Adv.* 6 (2016) 106485–106490, <https://doi.org/10.1039/C6RA22191B>.
- [51] Y.X. Gan, Activated carbon from biomass sustainable sources, *C* 7 (2021) 39, <https://doi.org/10.3390/c7020039>.
- [52] K. Liang, et al., Synthesis of nitrogen-doped mesoporous carbon for high-performance supercapacitors, *New J. Chem.* 43 (6) (2019) 2776–2782, <https://doi.org/10.1039/C8NJ05938A>.
- [53] L. Wan, et al., Nitrogen, sulfur co-doped hierarchically porous carbon from rape pollen as a high-performance supercapacitor electrode, *Electrochim. Acta* 311 (2019) 72–82, <https://doi.org/10.1016/j.electacta.2019.04.106>.
- [54] F. Dang, W. Zhao, P. Yang, H. Wu, Y. Liu, Nitrogen and sulfur co-doped hierarchical graphene hydrogel for high-performance electrode materials, *J. Appl. Electrochem.* 50 (4) (2020) 463–473, <https://doi.org/10.1007/s10800-020-01404-5>.
- [55] B. Mei, O. Munteshari, J. Lau, B. Dunn, L. Pilon, Physical Interpretations of Nyquist Plots for EDLC Electrodes and Devices, 2018, <https://doi.org/10.1021/acs.jpcc.7b10582>.
- [56] G. Wang, J. Zhang, S. Kuang, J. Zhou, W. Xing, S. Zhuo, Nitrogen-doped hierarchically porous carbon as an efficient electrode material for supercapacitors, *Electrochim. Acta* 153 (2015) 273–279, <https://doi.org/10.1016/j.electacta.2014.12.006>.
- [57] W. Fan, H. Zhang, H. Wang, X. Zhao, S. Sun, J. Shi, M. Huang, W. Liu, Y. Zheng, P. Li, Dual-doped hierarchical porous carbon derived from biomass for advanced supercapacitors and lithium-ion batteries, *RSC Adv.* 9 (2019) 32382–32394, <https://doi.org/10.1039/c9ra06914c>.